Automation and Machine Learning (2024)
Clausius Scientific Press, Canada

DOI: 10.23977/autml.2024.050206
ISSN 2516-5003 Vol. 5 Num. 2

Design of Autopilot Event-Triggered Control Systems

Ang Zheng[1,a,*], Yizhong Ding[1,b], Xiaoming Xia[2,c]

[1]Makarov College of Marine Engineering, Jiangsu Ocean University, Lianyungang, Jiangsu, China
[2]College of Marine Engineering, Jiangsu Ocean University, Lianyungang, Jiangsu, China
[a]2022221712@jou.edu.cn, [b]dingyizhong123@163.com, [c]xiaxiaoming@jou.edu.cn
[*]Corresponding author

Keywords: Autopilot, Extended state observer, Auxiliary dynamic system, Event-triggered control

Abstract: Addressing the challenges of designing unmanned ship autopilot control systems in a variable marine environment, this study proposes an anti-disturbance control method based on disturbance estimation and compensation under an event-triggered mechanism. The disturbances faced by unmanned ships are modeled as a first-order Nomoto process, capturing the marine disturbances caused by wind, waves, and currents as well as unmodeled dynamics. A extended state observer is constructed to estimate environmental disturbances and uncertainties within the ship model. In the control design, the estimated disturbances are used for compensation to mitigate the impacts of disturbances and uncertainties on the navigation control of unmanned ships. An auxiliary dynamic system is designed to reduce the effects of autopilot input saturation, and an event-triggered mechanism is introduced to decrease the frequency of autopilot actions to avoid excessive wear. Stability analysis using Lyapunov functions indicates that all error signals in the closed-loop system are bounded. Simulation results demonstrate the effectiveness and feasibility of the autopilot event-triggered control system.

1. Introduction

Under the influence of emerging technologies such as artificial intelligence and modern information technology, the navigation technology of unmanned ships is advancing rapidly towards intelligence and automation. The methods of using unmanned ships for water operations are becoming increasingly diverse. Unmanned ships can be used for a variety of tasks including water environment monitoring, scientific research exploration, surveying and mapping, as well as rescue operation [1]. During navigation, unmanned ships are affected by maritime conditions such as wind, waves, and currents, which can cause the vessel to deviate from its preset course, resulting in trajectory deviations and the inability to complete the anticipated tasks [2]. In response to this need, the autopilot control system has been developed to adjust the ship's heading in real-time during surface navigation [3], aiming to achieve intelligent and automated ship control. This enables the unmanned ship to navigate as closely as possible to the target course.

The autopilot is a maneuvering control device for ships, capable of calculating the necessary rudder angle based on heading errors to perform trajectory tracking control for unmanned ships. In [4], Sperry utilized a gyrocompass to measure the actual heading of the ship and employed a

feedback control method to complete the design of the first autopilot control system. Nicholas Minorsk [5] applied the Proportional-Integral-Derivative (PID) control algorithm to autopilot control systems. Banazadeh et al. [6] employed frequency domain identification techniques to recognize the model parameters of patrol boats and designed a PID autopilot controller. However, these studies did not consider the nonlinear maneuvering characteristics of ships. Addressing the nonlinear maneuvering characteristics of ships, Perera et al. [7] utilized input-output linearization techniques. They divided the ship motion system into linear dynamics and internal dynamics, designing a ship heading controller based on Lyapunov analysis methods. The literature [8]implemented a discontinuous control strategy to achieve finite-time stability in the ship heading control system and subsequently designed a global finite-time method for ship heading control that could converge rapidly. These studies did not fully consider the uncertain characteristics of the ship model, and due to factors such as onboard load, speed, and external environment, there were uncertainties during the ship's navigation. In [9] an observer with global exponential stability was constructed to estimate marine environmental disturbances online and designed a multi-ship synchronous formation control strategy with disturbance compensation capabilities. In [10], a robust nonlinear disturbance observer was designed to estimate and compensate for time-varying marine environmental disturbances, subsequently devising a synchronous navigation tracking control strategy for underactuated ships. Ning Jun et al. [11] developed an extended state observer to estimate the effects of time-varying marine environmental disturbances and designed a finite-time formation control strategy for unmanned ships.

Currently, control methods based on disturbance estimation and compensation are gaining increasing attention. The fundamental concept involves using an observer to estimate external disturbances and provide compensation. By integrating theories of disturbance estimation with fixed-time control [12], adaptive neural network control [13], $H\infty$ control [14], and variable structure control [15], methods for simultaneous cancellation and suppression of multiple sources of disturbances have been developed to achieve finely tuned disturbance resistance in control systems. Due to the physical limitations of ship systems, the rudder angle provided is affected by saturation constraints. Designing ship navigation control strategies that consider environmental disturbances and rudder angle saturation constraints aligns more closely with practical requirements.

To prevent excessive wear on the servo mechanisms, an event-triggered mechanism is applied to the autopilot control system. The core idea relies on pre-set triggering conditions, whereby the controller signal is updated only when these conditions are met, thus reducing excessive wear on the servo. Zhu et al. [16] designed a ship navigation event-triggered adaptive neural network fault-tolerant tracking control strategy, incorporating an auxiliary dynamic system to mitigate the effects of propulsion saturation constraints. They employed an upper bound disturbance adaptation method to suppress the impact of time-varying environmental disturbances on the control system, enhancing its disturbance resistance capabilities under varying conditions. However, this method relies on the error variables of executed actions and still exhibits disadvantages such as high frequency of actuator operations. In practical navigation, to reduce wear on actuators, the frequency of rudder movements is kept very low. Therefore, there is an urgent need to design a new type of trigger controller that significantly reduces the frequency of actuator actions, making the controller more suitable for engineering applications.

This paper proposes an autopilot control system under event-triggering, addressing the environmental disturbances and rudder angle input saturation issues encountered during unmanned ship navigation. Considering the marine environmental disturbances caused by wind, waves, and currents, a disturbance observer is constructed to estimate disturbances and uncertainties online. An auxiliary dynamic system reduces the impact of rudder angle saturation on the control system, and an event-triggering mechanism decreases the frequency of actuator operations to avoid excessive

wear on the ship's steering gear. Subsequently, using a Lyapunov function for stability analysis, it is shown that all error signals in the closed-loop system are bounded. Simulation results demonstrate the effectiveness of this method.

The structure of this paper is organized as follows: Section 1 establishes the unmanned ship model and formulas. Section 2 describes the design of the extended state observer. Section 3 introduces the design of the controller using an event-triggered and auxiliary dynamic system, provides stability analysis, and verifies the feasibility of the proposed control scheme. Section 4 provides a simulation to illustrate the theoretical results. Section 5 summarizes the paper.

2. Mathematical Model

2.1. Symbols

The following symbols will be used throughout this paper. $|\circ|$ represents absolute values, unless otherwise specified. $\|\circ\|$ represents the Euclidean norm. $R^{m\times n}$ represents the $m\times n$ dimensional Euclidean space. $\lambda_{\min}$ represents the minimum eigenvalue of a square matrix. $(\circ)^T$ represents the transpose of a matrix.

2.2. Model of the Ship

This ship motion is described by six degrees of freedom, namely surge, sway, yaw, heave, roll, and pitch. To simplify the complexity of ship motion control, only the motion in the horizontal plane, comprising the three degrees of freedom-surge, yaw, and sway-is typically considered. To quantitatively describe the motion of these three degrees of freedom, two coordinate systems are commonly used: one is the body-fixed frame, which takes the ship itself as the reference point; the other is the earth-fixed frame, which uses the earth as the reference point. As illustrated in Figure 1.

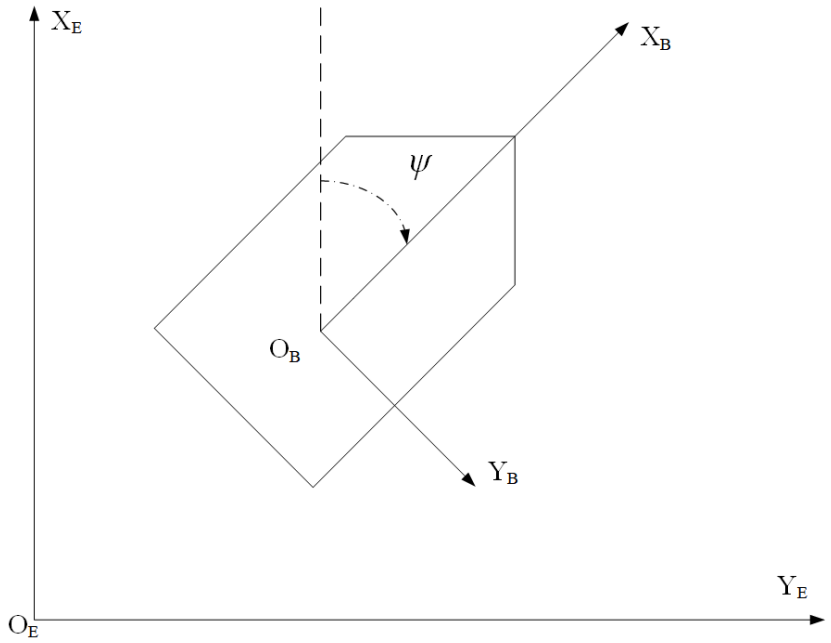

Figure 1: Earth-fixed frame $X_EO_EY_E$ and Body-fixed frame $X_BO_BY_B$

The mathematical model of an unmanned ship moving in the horizontal plane is described as follows [17]:

$$\begin{aligned}\dot{\eta} &= J(\psi)v \\ M\dot{v} &= -C(v)v - D(v)v + d + \tau\end{aligned} \tag{1}$$

Where $\eta = [x, y, \psi]^T$ is the vector of the ship position (x, y) and angle ψ heading in the earth-fixed frame. $v = [u, v, r]^T$ represents the vector of the ship velocities in surge, sway, and yaw in the body-fixed fram, $d = [d_1, d_2, d_3]^T$ represents the vector of environmental disturbances, $\tau = [\tau_u, \tau_v, \tau_r]^T$ is the control vector of the ship, including forces in surge τ_u, sway τ_v, and yaw moment τ_r. M is the inertia matrix, and D is the damping matrix. The matrices $J(\psi)$ are expressed as follows:

$$\begin{aligned} J(\psi) &= \begin{bmatrix} \cos(\psi) & -\sin(\psi) & 0 \\ \sin(\psi) & \cos(\psi) & 0 \\ 0 & 0 & 1 \end{bmatrix} \\ M &= \begin{bmatrix} m - X_{\dot{u}} & 0 & 0 \\ 0 & m - X_{\dot{v}} & mx_g - Y_{\dot{r}} \\ 0 & mx_g - N_{\dot{v}} & I_z - N_{\dot{r}} \end{bmatrix} \end{aligned} \tag{2}$$

In the formula, m represents the mass of the ship, I_z denotes the inertial moment of the ship about the axes of the body-fixed frame, x_g is the center of gravity of the ship in the body-fixed frame, and $X_{\dot{v}}$, $Y_{\dot{r}}$, $N_{\dot{v}}$, $N_{\dot{r}}$, represents the hydrodynamic parameters.

$$C = \begin{bmatrix} 0 & 0 & c_{13} \\ 0 & 0 & c_{23} \\ c_{31} & c_{32} & 0 \end{bmatrix} \tag{3}$$

Within the matrix: $c_{13} = -(m - X_{\dot{v}})v - (mx_g - Y_{\dot{r}})r$, $c_{23} = (m - X_{\dot{u}})u$, $c_{31} = (m - X_{\dot{v}})v + (mx_g - Y_{\dot{r}})r$, $c_{32} = -(m - X_{\dot{u}})u$. $C(v) = -C^T(v) \in R^{3\times3}$ represents the Coriolis-centripetal force matrix:

$$D = \begin{bmatrix} d_{11} & 0 & 0 \\ 0 & d_{22} & d_{23} \\ 0 & d_{32} & d_{33} \end{bmatrix} \tag{4}$$

Where $d_{11} = -(X_u + X_{u|u|}|u|)$, $d_{22} = -(Y_v + Y_{v|v|}|v| + Y_{r|v|}|r|)$, $d_{23} = -(Y_r + Y_{|v|r}|v| + Y_{|r|r}|r|)$, $d_{32} = -(N_v + N_{|v|v}|v| + N_{|r|v}|v|)$, $d_{33} = -(N_r + N_{|v|r}|v| + N_{|r|r}|r|)$, X_u, $X_{u|u|}$, Y_v, $Y_{v|v|}$, $Y_{r|v|}$, Y_r, $Y_{|v|r}$, $Y_{|r|r}$, N_v, $N_{|v|v}$, $N_{|r|v}$, N_r, $N_{|v|r}$, $N_{|r|r}$ is the hydrodynamic drag coefficient.

2.3. Model Decoupling

The mathematical model represented by equation (1) can be simplified by assuming a constant surge velocity $u = u_0$, resulting in a sway-yaw dynamics model, described as:

$$M_{vr}\dot{v}_{vr} + N(u_0)v_{vr} = \tau_{vr} \tag{5}$$

Where $v_{vr} = [v, r]^T$ is the state vector and τ_{vr} represents the vector of forces and moments in the sway and yaw directions respectively.

$$\begin{aligned} M_{vr} &= \begin{bmatrix} m - X_{\dot{v}} & mx_g - Y_{\dot{r}} \\ mx_g - N_{\dot{v}} & I_z - N_{\dot{r}} \end{bmatrix} \\ N(u_0) &= \begin{bmatrix} -Y_v & -Y_r + (m - X_{\dot{u}})u_0 \\ -N_v + (X_{\dot{u}} - Y_{\dot{v}})u_0 & -N_r + (mx_g - Y_{\dot{r}})u_0 \end{bmatrix} \end{aligned} \tag{6}$$

$N(u_0)$ can be expressed as:

$$N(u_0) = C_{vr} + D_L \tag{7}$$

Where:

$$\begin{aligned} C_{vr} &= \begin{bmatrix} 0 & (m - X_{\dot{u}})u_0 \\ (X_{\dot{u}} - Y_{\dot{v}})u_0 & (mx_g - Y_{\dot{r}})u_0 \end{bmatrix} \\ D_L &= \begin{bmatrix} -Y_v & -Y_r \\ -N_r & -N_r \end{bmatrix} \end{aligned} \tag{8}$$

Where:

$$\tau_{vr} = b\delta \tag{9}$$

Where $b = [-Y_\delta, -N_\delta]^T$, Y_δ and N_δ are the sway moment coefficient and yaw moment coefficient, respectively.

In this model, equation (5), considering only the motion in sway and yaw degrees of freedom, can be transformed into a Nomoto model:

$$\frac{r(s)}{\delta(s)} = \frac{K(1 + T_3 s)}{(1 + T_1 s)(1 + T_2 s)} \tag{10}$$

Where T_i $(i = 1, 2, 3)$ is related to the ship's following performance index, r is the heading angular velocity, δ is the rudder angle, and K is the ship's turning performance index.

Experimental results indicate that the constants T_2 and T_3 are almost equal [18]. Therefore, equation (10) can be written as:

$$\frac{r(s)}{\delta(s)} = \frac{K}{1 + Ts} \tag{11}$$

in the equation, $T = T_1 + T_2 - T_3$.

Considering saturation issues, and it can be attained that $-U_m \le \delta \le U_m$, U_m is the maximum rudder deflection. The error function between unsaturated and saturated problems is defined as $\sigma = \delta_c - \delta$, where δ_c is the rudder angle calculated by the controller.

2.4. Control Objective

The desired heading angle ψ_d provided by the system, and the desired heading angular velocity r_d, is obtained from the following second-order filter:

$$\begin{aligned}\dot{\psi}_a &= r_d \\ \dot{r}_d &= l_1^2(\psi_a - \psi_d) - 2l_1 r_d\end{aligned} \tag{12}$$

Where $l_1 \in R$ is a positive constant.

The control objective is to force the unmanned ship to track the reference heading signal ψ_d and reduce the frequency of servo actions, such that:

$$\lim_{t\to\infty} |\psi - \psi_d| \le \varepsilon \tag{13}$$

Where ε is a sufficiently small positive constant.

For clarity, the proposed controller structure diagram is provided below. As shown in Figure 2.

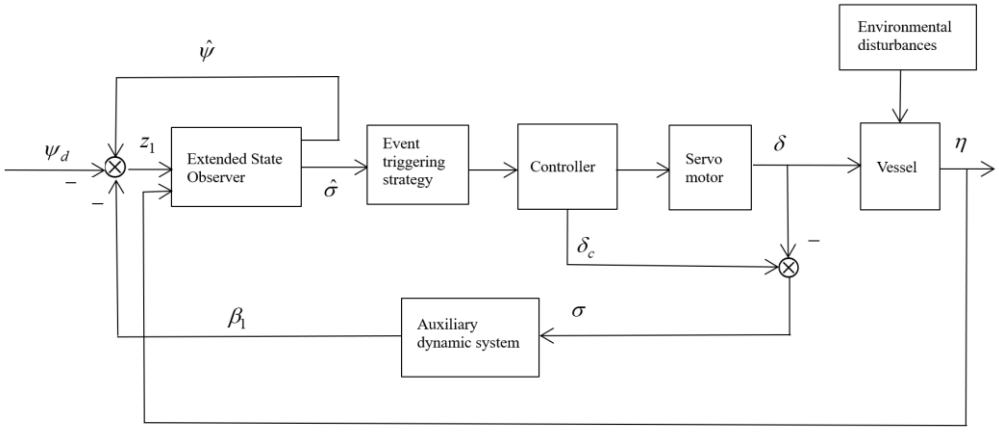

Figure 2: Structure diagram of the autopilot event-triggered control system

3. Extended State Observer

Due to the environmental disturbances and model uncertainties that the unmanned ship is autopilot control system encounters in practical operations, which are unknown and unmeasurable, an extended state observer is introduced to estimate the unknown environmental disturbances and model uncertainty information, thereby providing more accurate signals. Based on equation (11), the controller is designed as follows:

$$\dot{r} = \frac{K}{T}(\delta_c - \sigma + \delta_w) - \frac{1}{T}r \tag{14}$$

Where δ_w represents unknown but bounded environmental disturbance.

To facilitate the design of the extended state observer, we rewrite equation (14) in the state space form:

$$\begin{aligned}\dot{x}_1 &= x_2 \\ \dot{x}_2 &= x_3 + a + b_0 u_t \\ \dot{x}_3 &= h\end{aligned} \tag{15}$$

In the equation, $x_1 = \psi$, $x_2 = r$, $x_3 = (K/T)\delta_w$, $a = -(1/T)r$, $b_0 = (K/T)$, $u_t = \delta_c - \sigma$.

Assumption 1: There exists a positive constant h^* satisfying $\|h\| \le h^*$.

Remark 1: Assumption 1 is reasonable because the assumed environmental disturbances are bounded. a represents the controlled object, x_3 represents the environmental disturbances, h

represents the derivative of the environmental disturbances, and u_t is the input signal.

In expression (15), the matrix form can be expressed as follows:

$$\dot{x} = Ax + Bu + Eh \tag{16}$$

Where $x = [x_1, x_2, x_3]^T$ is the extended state vector.

$$A = \begin{bmatrix} 0 & 1 & 0 \\ 0 & -\frac{1}{T} & 1 \\ 0 & 0 & 0 \end{bmatrix}$$

$$B = \begin{bmatrix} 0 \\ b_0 \\ 0 \end{bmatrix} \tag{17}$$

$$E = \begin{bmatrix} 0 \\ 0 \\ 1 \end{bmatrix}$$

The estimated state of the state observer is as follows:

$$\dot{\hat{x}} = A\hat{x} + Bu + Le \tag{18}$$

Where $e = x_1 - \hat{x}_1$, $\hat{x} = [\hat{x}_1, \hat{x}_2, \hat{x}_3]^T$ is the estimation of x, $L = [k_1, k_2, k_3]^T$ is observer gain matrix with k_i, $(i = 1,2,3)$ is a positive constant.

Subtracting equation (18) from equation (16) yields the observation error for the state observer, as follows:

$$\dot{\tilde{x}} = A\tilde{x} + Eh - Le \tag{19}$$

In the equation, $\tilde{x} = x - \hat{x}$.

Define that $Le = LC\tilde{x}$, $C = [1,0,0]$. Therefore, equation (19) can be rewritten as:

$$\dot{\tilde{x}} = (A - LC)\tilde{x} + Eh \tag{20}$$

Option for an appropriate matrix L to stabilize the matrix $A - LC$. Under Assumption 1, equations (20) and (18) ensure that the estimates of environmental disturbances and model uncertainties converge to their true values within a finite time.

4. Controller Design

Before designing the controller, construct an auxiliary dynamic system to address the issue of servo input saturation. The auxiliary dynamic system is designed as [19]:

$$\dot{\beta}_1 = -L_1\beta_1 + \beta_2 \tag{21}$$

$$\dot{\beta}_2 = -L_2\beta_2 - b_0\sigma \tag{22}$$

Where L_1, L_2 is a positive constant, β_1, β_2 representing the auxiliary state.

The design process for the controller is as follows:

Step 1: Define the first error vector as:

$$z_1 = \hat{\psi} - \psi_d - \beta_1 \tag{23}$$

And select a Lyapunov function:

$$V_1 = \frac{1}{2} z_1^2 \tag{24}$$

According to equations (23) and (21), the time derivative of V_1 can be represented as:

$$\dot{V}_1 = z_1 \dot{z}_1 = z_1(\hat{r} - r_d + L_1\beta_1 - \beta_2) \tag{25}$$

Where $\hat{r}$ is the estimate of r.
Define the second error vector as:

$$z_2 = \hat{r} - \bar{\alpha} - \beta_2 \tag{26}$$

Where $\bar{\alpha}$ is a signal produced by a first-order low-pass filter, $l_2\dot{\bar{\alpha}} + \bar{\alpha} = \alpha$, where l_2 is a positive constant and α is a virtual control, defined as:

$$\alpha = -c_1 z_1 + r_d - L_1\beta_1 \tag{27}$$

Where $c_1 > 0$ is a constant.
Simplifying and combining equations (25) and (27) yields:

$$\dot{V}_1 = -c_1 z_1^2 + z_1(z_2 + \tilde{\alpha}) \tag{28}$$

In the equation, $\tilde{\alpha} = \bar{\alpha} - \alpha$.
Step 2: Select the Lyapunov function as follows:

$$V_2 = V_1 + \frac{1}{2} z_2^2 \tag{29}$$

Based on equations (18), (22), and (26), it follows that:

$$\dot{z}_2 = -\frac{1}{T}\hat{x}_2 + \hat{x}_3 + b_0(\delta_c - \sigma) - k_2 e - \dot{\bar{\alpha}} + L_2\beta_2 + b_0\sigma \tag{30}$$

Substituting equation (30) into the time derivative of V_2, and simplifying with equation (28) yields:

$$\dot{V}_2 = -c_1 z_1^2 + z_1(z_2 + \tilde{\alpha}) + z_2(-\frac{1}{T}\hat{x}_2 + \hat{x}_3 + b_0\delta_c - k_2 e - \dot{\bar{\alpha}} + L_2\beta_2) \tag{31}$$

To ensure z_2 stability, the controller is designed as:

$$\delta_c = \frac{1}{b_0}(-z_1 + \frac{1}{T}\hat{x}_2 - \hat{x}_3 + \dot{\bar{\alpha}} - c_2 z_2 - L_2\beta_2) \tag{32}$$

Where c_2 is a positive constant.
Substituting equation (32) into equation (31) results in:

$$\dot{V}_2 = -c_1 z_1^2 - c_2 z_2^2 + z_1\tilde{\alpha} - k_2 z_2 e \tag{33}$$

It is known from the literature [20], that $\tilde{\alpha}$ is bounded. $\tilde{\alpha}_u$ is the upper bound of $\tilde{\alpha}$. Using Young's inequality, we obtain:

$$z_1\tilde{\alpha} \le z_1\tilde{\alpha}_u \le \frac{1}{2}z_1^2 + \frac{1}{2}\tilde{\alpha}_u^2 \tag{34}$$

$$z_2 e \le \frac{1}{2}z_2^2 + \frac{1}{2}e^2 \le \frac{1}{2}z_2^2 + \frac{1}{2}\tilde{x}^T\tilde{x} \tag{35}$$

Step 3: Consider the total Lyapunov function as:

$$V = V_2 + \frac{1}{2}\beta_1^2 + \frac{1}{2}\beta_2^2 + \frac{1}{2}\tilde{x}^T\tilde{x} \tag{36}$$

The time derivative of V according to equations (20), (21), (22), (34), and (35) yields the following result:

$$\begin{aligned}\dot{V} \le &-(c_1 - \frac{1}{2})z_1^2 - (c_2 - \frac{k_2}{2})z_2^2 - (c_3 - \frac{k_2}{2})\tilde{x}^T\tilde{x} \\ &-L_1\beta_1^2 - L_2\beta_2^2 + \beta_1\beta_2 - b_0\beta_2\sigma + h^* + \frac{1}{2}\tilde{\alpha}_u^2\end{aligned} \tag{37}$$

Where $c_3 = \lambda_{\min}(A - LC)$, and $h*$ is given according to $\|Eh\| \le h*$.

Define $\bar{\sigma}$ as the upper bound of σ, and using Young's inequality, we obtain:

$$\begin{aligned}\beta_2\sigma \le \beta_2\bar{\sigma} \le \frac{1}{2}\beta_2^2 + \frac{1}{2}\bar{\sigma}^2 \\ \beta_1\beta_2 \le \frac{1}{2}\beta_1^2 + \frac{1}{2}\beta_2^2\end{aligned} \tag{38}$$

Hence, equation (37) can be written as:

$$\begin{aligned}\dot{V} \le &-(c_1 - \frac{1}{2})z_1^2 - (c_2 - \frac{k_2}{2})z_2^2 - (c_3 - \frac{k_2}{2})\tilde{x}^T\tilde{x} \\ &-(L_1 - \frac{1}{2})\beta_1^2 - (L_2 - \frac{1}{2} - \frac{b_0}{2})\beta_2^2 + \mu_1\end{aligned} \tag{39}$$

Where $\mu_1 = h^* + (1/2)\tilde{\alpha}_u^2 + (b_0/2)\bar{\sigma}^2$.

Step 4: In common continuous control schemes, the design has already been completed in Step 3. This paper adopts the concept of event-trigger control and establishes the triggering conditions will be established in this step. During the flow period between two consecutive trigger moments, a zero-order hold is used to maintain δ_c constant. The key to a successful event-triggered controller design lies in selecting an appropriate triggering condition. The current triggering moment is denoted as t_{g_i}, and the next triggering moment is determined by satisfying $t_{g_{i+1}}$ the following condition:

$$t_{g_{i+1}} = \inf\{t \in R \,|\, t > t_{g_i} \wedge W_a \ge \gamma V\} \tag{40}$$

Where $W_a = (c_1 - (1/2))z_1^2 + (c_2 - (k_2/2))z_2^2$, $0 < \gamma < \lambda_{\min}\{(c_1 - (1/2)), (c_2 - (k_2/2))\}$ are adjustable variables. Once the triggering condition is satisfied, thus $W_a \le \gamma V$, and it renders.

$$0 > -W_a > -\gamma V \tag{41}$$

And it implies $-W_a$ is bounded: Thus, we obtain:

$$\begin{aligned} \dot{V} &\le -W_a - (c_3 - \frac{k_2}{2})\tilde{x}^T\tilde{x} - (L_1 - \frac{1}{2})\beta_1^2 - (L_2 - \frac{1}{2} - \frac{b_0}{2})\beta_2^2 + \mu_1 \\ &\le -(c_3 - \frac{k_2}{2})\tilde{x}^T\tilde{x} - (L_1 - \frac{1}{2})\beta_1^2 - (L_2 - \frac{1}{2} - \frac{b_0}{2})\beta_2^2 + \mu_1 \end{aligned} \tag{42}$$

From the definition of V, it can be determined that V, $\tilde{x}$, β_1, β_2 are bounded and convergent. It is known from the $W_a \le \gamma V$ that z_1, z_2 are bounded. The above proof demonstrates that V is convergent, and thus z_1, z_2 is also convergent. Therefore, all signals in the closed loop are bounded.

Thus, equation (42) can be written as:

$$\dot{V} \le -cV + \mu_1 \tag{43}$$

Where c is a positive constant.

If the triggering condition is met, $c = \lambda_{\min}\{(c_3 - (k_2/2)),\ (L_1 - (1/2)),\ (L_2 - (1/2) - (b_0/2))\}$, otherwise $c = \lambda_{\min}\{(c_1 - (1/2)),\ (c_2 - (k_2/2)),\ (c_3 - (k_2/2)),\ (L_1 - (1/2)),\ (L_2 - (1/2) - (b_0/2))\}$.

Ultimately, it can be derived that:

$$V(t) \le (V(0) - \frac{\mu_1}{c-\gamma})e^{-(c-\gamma)t} + \frac{\mu_1}{c-\gamma} \tag{44}$$

Based on the definition of V, it can conclude that z_1, z_2, $\tilde{x}$, β_1, and β_2 are bounded. From equation (44), z_1 exponentially converges to a compact set $\Pi = \{z_1 \,|\, |z_1| \le 2(\mu_1/(c-\gamma))\}$ that can be made arbitrarily small by adjusting $c-\gamma$, it can be maintained $\lim_{t\to\infty}|\psi - \psi_d| \le \varepsilon$, thus completing the control over the controlled object.

5. Simulation Results

This section conducts simulations using Matlab and provides simulation results to verify the effectiveness and feasibility of the controller. The parameters for the extended state observer are set $k_1 = 4$, $k_2 = 5$, $k_3 = 10$, and the range $|\delta| \le 35^\circ$ for the rudder angle is established. The sampling period for the triggering condition is $0.01s$, $t_{g_{i+1}} - t_{g_i} = 0.01$, $\gamma = 0.01$. with the reference heading signal set to $\psi_d = 30^\circ$, $0s \le t \le 250s$. when $\psi_d = 0^\circ$, $250s \le t \le 500s$.

Figure 3 depicts the output response of the controller, where the blue solid line represents the desired output heading angle, the red solid line indicates the actual heading angle signal under the event-triggered control system, and the black dashed line shows the estimated heading angle curve. As seen in the figure, the event-triggered control system allows the unmanned ship to accurately track the reference course, achieving the expected tracking performance. In Figure 4, the blue solid line represents the heading angular velocity, and the red dashed line shows the estimated heading angular velocity curve. It can be observed that the event-triggered control system achieves good estimation results even when the heading angular velocity is unknown, and the estimation of the heading angular velocity converges well to the actual heading angular velocity. Figure 5's blue solid line represents environmental disturbances, and the red solid line shows the estimation of these disturbances. The results demonstrate that the state observer can accurately estimate environmental disturbances. Figure 6 displays the variation over time of the rudder angle δ under

the event-triggered control system conditions. From the figure, it is evident that the frequency of rudder angle updates is significantly lower than that achieved by traditional time-sampling methods. The event-triggered control system reduces mechanical wear and fuel consumption by lowering the frequency of autopilot usage.

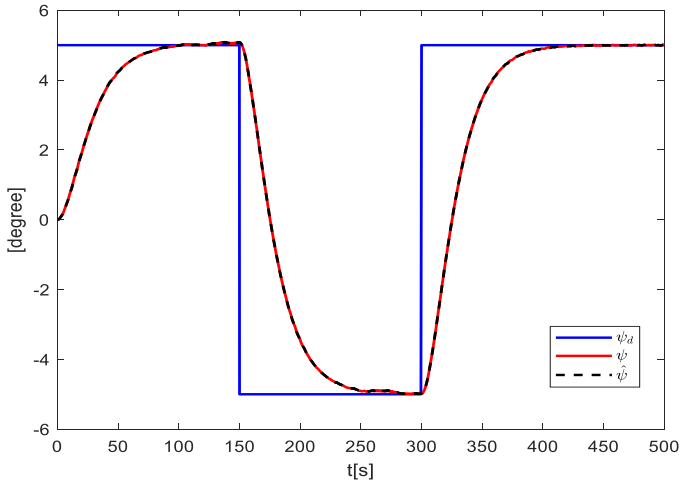

Figure 3: Heading-tracking curve

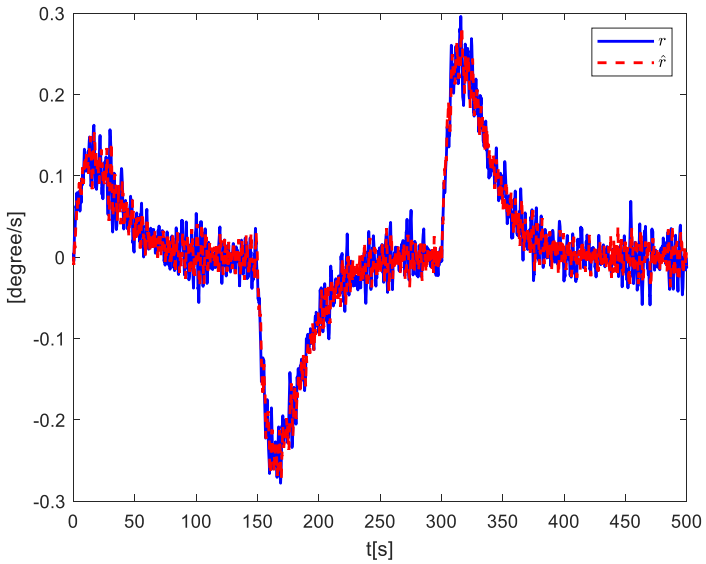

Figure 4: Heading angle velocity and its estimated curves

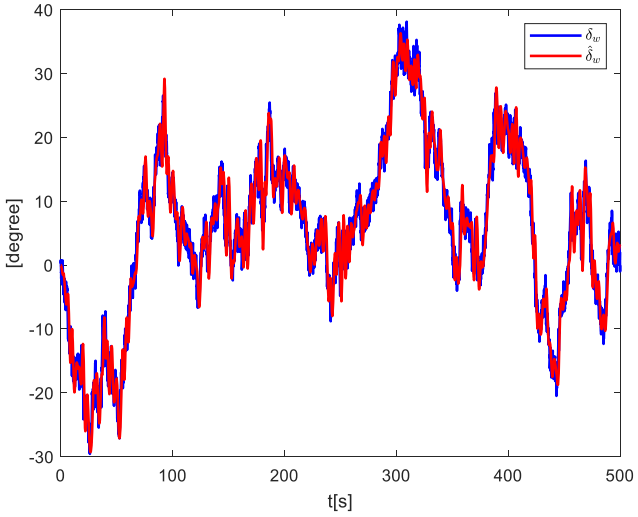

Figure 5: Environmental disturbances and their estimated curves

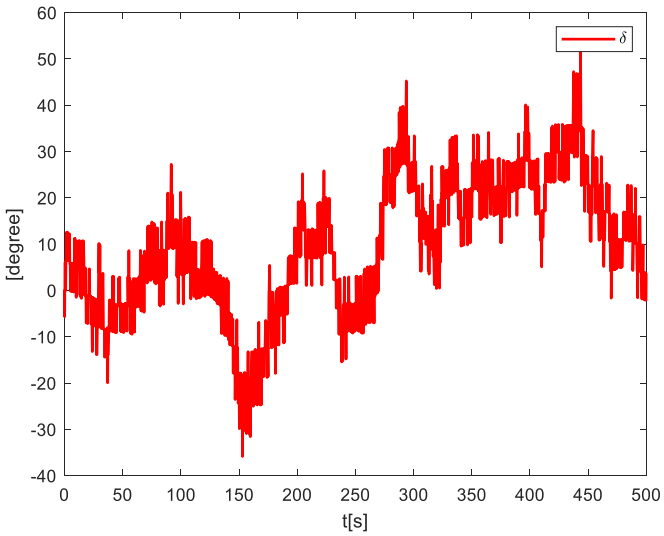

Figure 6: Steering angle curve under the event-triggered control condition

6. Conclusion

This paper conducts an in-depth study on the autopilot control problem for unmanned ships, particularly addressing issues related to environmental disturbances and servo input saturation. A control strategy based on extended state observer, auxiliary dynamic systems, and event-triggered is proposed. An extended state observer is utilized to estimate unknown environmental disturbances as well as model uncertainties. An auxiliary dynamic system is employed to handle saturation issues. The final derivation of the event-triggered conditions ensures that the autopilot controller updates only when these conditions are met, significantly reducing mechanical wear and fuel consumption. Simulation results demonstrate that the designed controller can ensure the unmanned ship's actual heading accurately tracks the reference heading. Stability analysis based on Lyapunov's theorem proves that all signals are bounded, and the tracking error converges to a neighborhood of the origin. The feasibility of the proposed control algorithm is validated using Matlab simulations.

References

[1] Yu H. An Autonomous Obstacle Avoidance System for Unmanned Ship Navigation with Improved Artificial Potential Field Method [J]. Ship Science and Technology, 2023, 45 (20): 97-100.

[2] Huang Z. Design and Implementation of Tracking Control System for Measuring Ships [D]. Tianjin University, 2022.

[3] Jiang Yudong. Design and Optimization of Autonomous Rudder Control System for Unmanned Ships [D]. Dalian University of Technology, 2020.

[4] Fossen T I. Handbook of marine craft hydrodynamics and motion control [M]. West Sussex: Wiley, 2011.

[5] O. H F. Discussion: "Note on Angular Motions of Ships" (Minorsky, Nicholas, 1941, ASME J. Appl. Mech., 8, pp. A111–A120) [J]. J. Appl. Mech, 1942, 9(2): A100-A112.

[6] Banazadeh A, Ghorbani M T. Frequency domain identification of Nomoto model to facilitate Kalman filter estimation and PID heading control of a patrol vessel [J]. Ocean Engineering, 2013, 72: 344-355.

[7] Perera L P, Soares C G. Lyapunov and Hurwitz based controls for input-output linearization applied to non linear vessel steering [J]. Ocean Engineering, 2013, 66: 58-68.

[8] Wang N, L ü S L, Liu Z Z. Global finite-time heading control of surface vehicles[J]. Neurocomputing, 2016, 175: 662-666.

[9] DO K D. Synchronization motion tracking control of multiple underactuated ships with collision avoidance [J]. IEEE Transactions on Industrial Electronics, 2016, 63(5): 2976-2989.

[10] HU X, WEI X J, KAO Y G, et al. Robust synchronization for under-actuated vessels based on disturbance observer [J]. IEEE Transactions on Intelligent Transportation Systems, 2022, 23(6): 5470-5479.

[11] NING J, CHEN H M, LI W, et al. Finite-time ship formation control based on extended state observer [J]. Chinese Journal of ShipResearch, 2023, 18 (1): 60-66.

[12] LIU Y, JIA H C, LIU L, et al. Anti-disturbance optimal coverage control of ASVs[J]. Chinese Journal of Ship Research, 2023, 18 (1): 67-77.

[13] ZHANG R, XU B, SHI P. Output feedback control of micromechanical gyroscopes using neural networks and disturbance observer [J]. IEEE Transactions on Neural Networks and Learning Systems, 2022, 33(3): 962-972.

[14] LI L Y, PEI G J, LIU J X, et al. 2-DOF robust H∞ control for permanent magnet synchronous motor with disturbance observer[J]. IEEE Transactions on Power Electronics, 2021, 36(3): 3462-3472G.

[15] YIM J, YOU S, LEE Y, et al. Chattering attenuation disturbance observer for sliding mode control: application to permanent magnet synchronous motors [J]. IEEE Transactions on Industrial Electronics, 2023, 70(5): 5161-5170.

[16] ZHU G B, MA Y, LI Z X, et al. Event-triggered adaptive neural fault-tolerant control of underactuated MSVs with input saturation [J]. IEEE Transactions on Intelligent Transportation Systems, 2022, 23(7): 7045-7057.

[17] Fossen T I, Marine Control Systems, Marine Cybernetics, Trondheim, Norway, 2002.

[18] Zhang G, Zhang X, Mathematical Model of Ship Motion and MATLAB Simulation [M] Xuzhou: China University of Mining and Technology Press, June 47-50, 2020.

[19] G. Xia, C. Sun, B. Zhao, X. Xia, and X. Sun, Neuroadaptive distributed output feedback tracking control for multiple marine surface vessels with input and output constraints, IEEE Access, 2019, 7: 123076–123085.

[20] G. Xia, C. Sun, B. Zhao, and J. Xue, Cooperative control of multiple dynamic positioning vessels with input saturation based on finite-time disturbance observer, International Journal of Control, Automation and Systems, 2019, 17(2): 370–379.